Effect of thermal cycling frequency on the durability of Yb-Gd-Y-based thermal barrier coatings

Guanlin Lyu[1], Baig-Gyu Choi[2], Zhe Lu[3], Hyeon-Myeong Park[1], Yeon-Gil Jung[*,1], Jing Zhang[*,4]

[1]School of Materials Science and Engineering, Changwon National University, Changwon, Gyeongnam 51140, Republic of Korea

[2]High Temperature Materials Research Group, Korea Institute of Materials Science, Changwon, Gyeongnam 51140, Republic of Korea

[3]School of Materials and Metallurgy, University of Science and Technology Liaoning, No. 185 High-Tech District, Anshan, Liaoning, 114051, China

[4]Department of Mechanical and Energy Engineering, Indiana University-Purdue University Indianapolis, Indianapolis, IN 46202, USA

This is the author's manuscript of the article published in final edited form as:

Lyu, G., Choi, B.-G., Lu, Z., Park, H.-M., Jung, Y.-G., & Zhang, J. (2019). Effect of thermal cycling frequency on the durability of Yb-Gd-Y-based thermal barrier coatings. Surface and Coatings Technology. https://doi.org/10.1016/j.surfcoat.2019.02.069

Abstract

The effects of thermal cycling frequency and buffer layer on the crack generation and thermal fatigue behaviors of Yb–Gd–Y-stabilized zirconia (YGYZ)-based thermal barrier coatings (TBCs) were investigated through thermally graded mechanical fatigue (TGMF) test. TGMF tests with low- (period of 10 min) and high-frequency (period of 2 min) cycling were performed at 1100 ^{o}C with a 60 MPa tensile load. Different cycling frequencies in TGMF test generate two kinds of crack propagation modes. The sample with low-frequency cycling condition shows penetration cracks in the YGYZ top coat, and multiple narrow vertical cracks are generated in high-frequency cycling. To enhance the thermomechanical properties, different buffer layers were introduced into the TBC systems, which were deposited with the regular (RP) or high-purity 8 wt% yttria stabilized zirconia (HP-YSZ) feedstock. The purity of the feedstock powder used for preparing the buffer layer affected the fracture behavior, showing a better thermal durability for the TBCs with the HP-YSZ in both frequency test conditions. A finite element model is developed, which takes creep effect into account due to thermal cycling. The model shows the high stresses at the interfaces between different layers due to differential thermal expansion. The failure mechanisms of YGYZ-based TBCs in TGMF test are also proposed. The vertical cracks are preferentially created, and then the vertical and horizontal cracks will be propagated when the vertical cracks are impeded by pores and micro-cracks.

Keywords: Thermal barrier coating; Buffer layer; Purity; Thermally graded mechanical fatigue test; Thermal frequency cycling

1. Introduction

Thermal barrier coatings (TBCs) are widely used in aircraft engines and land based gas turbines to protect the metallic substrates of hot-section components from high temperature environments. TBCs enhance the fuel efficiency by enabling higher temperature operations and extending lifetime performance of hot-section components in aircraft and gas turbine engines. For aircraft engines, many researches [1-4] have focused on the thermomechanical fatigue loadings which adversely influence the durability of TBCs, and their failure mechanisms. The ceramic top coat in a typical TBC system is made of 6–8 wt% yttria-stabilized zirconia (YSZ), which has low thermal conductivity, superior thermal stability and similar coefficient of thermal expansion (CTE) to metallic substrate. As the gas turbine inlet temperature increases (> 1200 °C), there is a concern about the current YSZ TBCs which are prone to the phase transformation and sintering, causing early delamination under high temperature environments [5]. Additionally, the hot-section components in a rotation part with TBC systems are subject to severe stresses conditions, such as cyclic thermal gradient and centrifugal force. Consequently, the TBCs and substrates experience cyclic thermal and mechanical loads in an engine environment, and their lifetime performance are limited by thermomechanical fatigue [6]. Therefore, the lifetime performance of the TBC systems should be evaluated in thermomechanical environments, especially for the TBCs applied to the hot-section component of a rotation part. Thermomechanical tests require appropriate control of both mechanical and thermal loading, and the thermal graded mechanical fatigue (TGMF) test has been believed to be an effective way to reproduce stress states close to service condition.

In terms of TBC materials, rare-earth zirconates ($Re_2Zr_2O_7$, Re = La, Gd, Eu, Dy)

are regarded as alternative ceramic materials to YSZ that have higher melting points (> 2000 °C), better phase stabilities, and lower thermal conductivities [7,8]. One of the candidates, $Gd_2Zr_2O_7$ has no volumetric phase transformation, unlike YSZ, and it undergoes an order–disorder transition; i.e., a transformation from a defect fluorite structure to a pyrochlore structure [9]. As another candidate for advanced TBC materials, zirconate material doped with lanthanum (La), ytterbium (Yb), gadolinium (Gd), yttrium (Y), or Yb–Gd–Y-stabilized zirconia (hereinafter YGYZ), has been proposed for more stable TBCs [10–12]. YGYZ coating has several advantages compared with YSZ coating in terms of its thermomechanical and thermochemical properties, such as better oxidation resistance, improved sintering resistance, higher calcium–magnesium–alumina–silicate resistance, excellent phase stability, and lower thermal conductivity. YGYZ has a thermal conductivity of 0.80–1.24 $W\cdot(m\cdot K)^{-1}$ in bulk form and of 2.1 $W\cdot(m\cdot K)^{-1}$ for bulk 8YSZ [13–16]. However, higher CTE mismatch and lower fracture toughness values were observed in $Gd_2Zr_2O_7$, which may cause coating's premature failures [17,18].

Consequently, a layered structure was believed as an effective way to overcome the bulk material's drawbacks. In particular, a multilayer concept has been recently proposed, which includes an erosion-resistant layer as an outer layer, a thermal barrier layer, a corrosion–oxidation-resistant layer, a thermal stress control layer, and a diffusion-resistant layer [19,20]. Additionally, regular and high purity YSZ buffer layers were introduced which can reduce the stresses generated at the interface due to the CTE mismatch during cyclic thermal exposure. Moreover, the mechanical property of ceramic top coat was improved by adding these buffer layers.

Given the discussions above, in this study, the goal is to understand the failure mechanisms of the layered YGYZ-based TBCs in the combined thermal and mechanical

environments, with a focus on the thermal cycling frequency and buffer layer purity effects. The TGMF test can simulate the cyclic mechanical loading and thermal gradient under operating conditions of rotating parts in turbines. Two different thermal cycling frequencies, 1/120 Hz (or 2 mins period, or high-frequency thereafter) and 1/600 Hz (or 10 mins period, or low-frequency thereafter), in the TGMF tests were employed. Additionally, the effects of buffer layers prepared with two different feedstock powders (regular- and high-purity powders or RP- and HP-YSZ thereafter) on the crack generation and thermal fatigue behaviors were investigated. Finally, the relationship between the thermal durability and buffer layer species in the YGYZ-based TBC systems was discussed, with a focus on the microstructural evolution in the TGMF tests.

2. Experiment procedure

2.1 Coating materials and sample preparation

The substrate was made of nickel superalloy with a thickness of approximately 5.5 mm. The side and surface photographs of the sample employed in the TGMF test are shown in Fig. 1. The feedstock of the bond coat was AMDRY 9951 (Sulzer Metco Holding AG, Wohlen, Switzerland). The bond coat was deposited on the nickel superalloy substrate by the high-velocity oxy-fuel (HVOF) process using a Diamond Jet-2600DJM (Sulzer Metco Holding AG). Two YSZ buffer layers were deposited on the bond coat using two feedstock powders (METCO 204C-NS with regular purity: $8.0Y_2O_3$-$0.7SiO_2$-$0.2TiO_2$-$0.2Al_2O_3$-$0.2Fe_2O_3$ doped in ZrO_2, hereinafter RP-YSZ and METCO 204C-XCL with high purity: $8.0Y_2O_3$-$0.05SiO_2$-$0.05TiO_2$-$0.05Al_2O_3$-$0.05Fe_2O_3$ doped in ZrO_2, hereinafter HP-YSZ; Sulzer Metco Holding AG), as shown in Fig. 2 (A) and (B), respectively. The YGYZ top coat was coated on each buffer layer using a commercial feedstock powder (METCO

206A: $9.5Y_2O_3$-$5.6Yb_2O_3$-$5.2Gd_2O_3$ doped in ZrO_2; Sulzer Metco Holding AG) with a size range of 45 to 125 μm, as shown in Fig. 2 (C). The buffer layer and top coat were sprayed following the air plasma spraying (APS) method using the 9 MB coating system (Sulzer Metco Holding AG). Based on the information provided by the powder supplier [21,22], the high-purity zirconia-based powders, such as HP-YSZ or METCO 204C-XCL, show improved high-temperature sintering resistance due to low concentrations of alumina and silica. Testing has shown that these high-purity systems show improved sintering characteristics, are less prone to phase and structural changes, and have better thermal-cyclic life.

The schematic diagrams of the layered TBC structural design proposed in this study are shown in Fig. 3. The thicknesses of the bond coat, buffer layer, and top coat were designed as 450 ± 50, 100 ± 20, and 800 ± 100 μm, respectively.

2.2 TGMF test

Crack generation and lifetime performance of the YGYZ-based TBCs were investigated in the combined mechanical and thermal environments. A photograph of the TGMF apparatus is shown in Fig. 4. The schematic illustration of flame shock on the TBC surface in the TGMF test is shown in Fig. 5(A), along with the applied tensile loading direction, and the applied tensile load was controlled by a load cell. The TGMF test uses liquid petroleum gas (LPG) as the fuel. The surface temperatures of tested samples are approximately 1100 °C during heating process. The samples are cooled in ambient air when the torch is retreated during cooling process.

Two different cycling frequencies of TGMF test, i.e., high-and low-frequency cycling (Fig. 5(B) and Fig.5(C), respectively), were employed, which correspond to the

high- and low-rotation of turbine engine starting process. In Figs. 5(B) and (C), the red solid and black dotted lines indicate the measured and scheduled temperatures, respectively. The temperatures on the surface and backside of TBC were measured by an infrared-temperature measurement device (wavelength: 3.9 μm, CTlaser MT; Optris, Berlin, Germany). A 60 MPa uniaxial tensile load (δ_a) was applied. The strain rate and total strain were controlled by a computerized control program at 1.5 mm/min and 0.2%, respectively.

In the low-frequency cycling condition, the samples were heated and cooled for 10 min in each cycle. In contrast, in the high-frequency cycling condition, the samples were heated and cooled for 2 min in each cycle. To keep the total thermal exposure time same (total 10,000 mins), the low- and high-frequency cycles were operated for 1,000 and 5,000 cycles, respectively. A summary of the numbers of cycles and total exposure time is shown in Table 1. The criteria that were adopted for failure in the TGMF tests were > 50% spalling of the region, or cracking in the top coat and/or at the interface.

2.3 Characterizations

To evaluate the microstructures of tested samples, the cross sectional views of selected regions were chosen, which are parallel to the tensile loads applied to the samples. Due to the flame shock's local concentrations shown in Fig. 5(A), only the center coverage of the samples were selected in this investigation. The selected samples were preprocessed to observe the cross-sectional microstructure before and after the TGMF tests. The samples were cold-mounted using epoxy resin, polished using silicon carbide paper, and then finally polished using 3 μm and 1 μm diamond pastes. The cross-sectional microstructures of the TBCs were observed using a scanning electron microscope (Model JSM-561; JEOL,

Tokyo, Japan) in backscattered electron image mode. Crack generation at the interface between the buffer layer and top coat, and the effect of tensile load on the samples in the thermal and mechanical environments were studied. Moreover, image analysis was conducted to measure the porosity of the cross-sectional microstructure images of the top coats.

2.4 Finite element model description

A finite element of the TBC structure subject to thermal cycling conditions was built. Due to axial symmetry, only a half cross-section with axial symmetric finite element was used for the model. The geometry of the TBC is identical to the experimental specimen.

The typical elastic materials properties for YGYZ, YSZ, bond coat, and nickel superalloy substrate were used. In order to understand the thermal cycling effect on the mechanical behavior of the coating, a creep model was also applied to the YGYZ layer. For the mechanical boundary conditions, the symmetric axis was imposed as axial symmetry. The bottom of the structure was applied with a roller condition. For thermal boundary conditions, the thermal cycling conditions identical to the experimental conditions in Table 1 were imposed.

3. Results and discussion

3.1. Characterization of as-prepared samples

The cross-sectional microstructures of two layered TBCs before the TGMF test are shown in Fig. 6. The TBCs did not show delamination or cracking at the interface between the top and bond coats. The top coats, buffer layers, and bond coats were well

deposited with the thicknesses of 816–833 μm, 106–117 μm, and 469–486 μm, respectively. However, the effect of the thickness differences is not considered in this investigation because its impact is negligible on thermal durability, according to the previous studies [23,24]. The porosity of the YGYZ top coat is 14.9%. The bond coat prepared by the HVOF process showed a dense microstructure and low oxide contents. A laminar structure was shown in the top coats, in which pores and micro-cracks were inevitable due to the internal thermal stress in the process of thermal spraying [25]. The orientation of the cracks and pores normal to the heat flow reduces the thermal conductivity of the top coat from ≈2.3 $W\cdot(m\cdot K)^{-1}$ for a fully dense material to a more typical 0.8 to 1.7 $W\cdot(m\cdot K)^{-1}$ [3]. In addition, the top coat and buffer layer were bound tightly due to the similar microstructure prepared by the same coating method.

3.2 Effect of thermal cycling frequency on TBC durability

The TGMF testing technique used in this study simplifies the original testing apparatus developed in the late 1990s, in order to facilitate the setup of the experiment and also sample preparation using a flat sample geometry [26,27]. The photographs of a tested sample and apparatus are shown in Figs. 1 and 4, respectively.

A summary of the number of cycles and exposure time in the TGMF tests is given in Table 1. Until the end of the TGMF tests (10,000 mins), no obvious delaminations were observed with a visual inspection in both cycling frequency conditions.

The overall microstructures of the TBCs with the buffer layer species after the TGMF tests are shown in Fig. 7. For the low- thermal cycling frequency (Fig. 7(A-1) and (B-1)), vertical cracks were generated that were perpendicular to the direction of the

tension load. The horizontal cracks were parallel to the interface between the bond and top coats, independent of the buffer layer species. In contrast, for the high thermal cycling frequency, multiple narrow cracks were observed (Fig. 7(A-2) and (B-2)). In addition, the porosities of the YGYZ top coats after low- and high-frequency TGMF test are 19.59% and 17.08%, respectively. Compare to as-prepared sample, the cracks generation caused the increasing of the porosity.

The TBCs in the high thermal cycling frequency showed notable differences in fracture resistance compared with the low thermal cycling frequency, independent of bond coat species. Two kinds of thermal cycling frequency in TGMF test generated different cracks patterns due to the temperature difference between the top coat and buffer layer. For the low thermal cycling frequency, the surface temperature of tested samples reached 1100 °C, and then cooled to 450 °C; while cooled to 700 °C for the high thermal cycling frequency, as shown in the actual temperature curves (solid lines) in Fig. 5(B) and (C). Therefore, the actual temperature difference of adjacent cycles in the high thermal cycling frequency was less than that in the low thermal cycling frequency, indicating that the temperature difference within the sample could not generate enough thermal and residual stresses to create cracks in the top coat. In addition, the magnitude of the thermal and residual stresses can be diffused quickly due to the narrow cracks near the surface, which is important for applications with relatively fast cooling/heating rates. In another word, the appearance of narrow cracks is beneficial to prevent the vertical cracks propagating during the process of stress relief. In our previous study [28], the blended LZO-YSZ based TBCs with RP-YSZ buffer layer generated more vertical cracks than YGYZ-based TBCs. Therefore, the YGYZ-based TBCs showed a better thermal durability in the low-frequency cycling TGMF test.

3.3 Effect of buffer layer purity on TBC durability

Highly magnified cross-sectional microstructures of samples tested with the low thermal cycling frequency are shown in Fig. 8. In the TBC with the buffer layer of RP-YSZ and HP-YSZ (Fig. 8(A) and (B)), vertical cracks propagated to the interface between the top coat and the buffer layer, and then transverse cracks were deflected above the buffer layer. The highly magnified cross-sectional microstructures of samples tested with the high thermal cycling frequency are shown in Fig. 9. After the TGMF test, the TBCs generated multiple narrow vertical cracks near the surface, as shown in Fig. 9(A-1) and (B-1). The vertical cracks propagated toward the interface between the top coat and the buffer layer.

In the TBC with the buffer layer of HP-YSZ (Fig. 8(B)), horizontal cracks were generated within the top coat and at the interface between the top coat and the buffer layer. The horizontal cracks at the interface between the buffer layer and the top coat, and/or between the bond and top coats indicate that the thermal and residual stresses were induced as a result of the CTE mismatch.

The CTE mismatch between the bond coat and the top coat was reduced by introducing the buffer layer, and the strain at the surface was also decreased. The thermal mismatch induced strain (ε) and stress (σ) during the TGMF test can be roughly calculated by Eqs. (1) and (2) as follows [29]:

$$\varepsilon = (\alpha_{Sub} - \alpha_{TC}) \times \left(\bar{T} - T_{surface}\right), \quad (1)$$

$$\sigma = E \times (\alpha_{Sub} - \alpha_{TC}) \times \left(\bar{T} - T_{surface}\right), \quad (2)$$

where α_{TC} and α_{Sub} are the CTEs of the top coat and the bond coat (CTE is 9–10 × 10^{-6} K^{-1} for bulk YGYZ, 10.5–11.5 × 10^{-6} K^{-1} for YSZ, and 15.0 × 10^{-6} K^{-1} for metallic bond coat at 1000 °C [30–32]), respectively, the $\bar{T}$ is the mean temperature in the top coat, and

the E is the elastic modulus of the ceramic materials. In our previous study [33], The E values which were measured by nano-indentation for YGYZ top coat, and the RP-YSZ and HP-YSZ buffer layers, which were determined to be 113.9 ± 23.8 GPa, 123.0 ± 23.8 GPa and 121.0 ± 21.7 GPa, respectively.

Using the above equations, one can briefly show that the thermal and residual stresses were developed due to the CTE mismatch at the interfaces between the buffer layer and the bond coat, leading to cracking at the interfaces of the TBCs. The ceramic part was subject to a tensile stress during heating and a compressive stress during cooling in the direction parallel to the interface. The reverse stress status was created in the perpendicular direction. The buffer layer provided localized stress relief due to its high strain compliance, which can delay the delamination of the TBC and therefore enhance its lifetime performance.

In summary, the samples with the HP-YSZ buffer layer have a better thermal and mechanical durability in the low-frequency TGMF test. The YSZ buffer layer prevented the propagation of the vertical cracks towards the interface between the top and bond coats, through reducing their CTE mismatch. Some researcher found that the HP-YSZ exhibited greater resistance to phase transformation (from T phase to M phase) at high temperatures [34]. For the low-frequency test, as shown in Figs. 8(A-3) and (B-3), some fine cracks were generated in both the RP- and HP-YSZ buffer layers. Even if vertical cracks were generated only in the RP-YSZ buffer layer, it is difficult to tell the statistical difference based on the microstructure. For the high-frequency test, the difference between the HP-YSZ and RP-YSZ is less evident, since the generated vertical cracks were far away from the buffer layer.

3.4 Finite element model results

The geometry and finite element mesh of the TBC are shown in Fig. 10. Convergence study was conducted to check the sufficiency of the mesh density. The von Mises stress distributions of in the TBCs are shown in Fig. 11. As seen in the figure, under both thermal cycling conditions, the maximum stresses occurred at the interfaces between different layers, due to differential thermal expansions. In general, the low-frequency sample had a slightly higher maximum stress than the high-frequency one, which was caused by a larger temperature difference in thermal cycling.

The effective creep strain evolutions at the outer edge of the YGYZ and YSZ interface are plotted in Fig. 12. For both thermal cycling conditions, the effective creep strains continued to increase with time. The high-frequency sample had a faster strain increase rate than the low-frequency one, which may cause potential delamination.

3.5 Mechanisms of fracture generations in the TBC in TGMF test

Thermal cycling frequency causes different crack generation modes with different lengths and quantities of the vertical cracks. The microstructural of the tested samples under low- and high thermal cycling frequency had different cracks generations. Fig. 13 (A) and (B) show the crack propagation models under low- and high thermal cycling frequency in the TGMF test, respectively. The sample generated a penetration crack in top coat under low thermal cycling frequency, indicated by a thick line in Fig. 13(A). But more narrow vertical cracks were generated near the surface under high-frequency cycling, indicated by thin lines in Fig. 13(B). No penetrating cracks were generated in YGYZ top coat, indicating that smaller thermal and residual stresses were exerted at the interface between the top coat (or buffer layer) and the bond coat. In addition, the 60 MPa tensile load applied to the samples in

the TGMF test enhanced the tensile stress on the surface. Therefore, vertical cracks were easily generated in the direction perpendicular to the load. When the vertical cracks have been impeded by pores and micro-cracks with enough energy (thermal and residual stress), the cracks will pass through the pores and micro-cracks and continue to propagate in top coats. The crack tended to propagate along the spray direction due to the tensile radial stress with a high magnitude and reaches to the interface between the ceramic and metallic layers [35]. Moreover, in Fig. 8 and 9, the TGO thickness are approximately 1~3 μm. Therefore, the TGO layers can be considered not affecting the cracks propagation and thermomechanical stability in this work. Horizontal cracks were easily generated at the interface among the splats boundary in TBC prepared by the APS process, which can be attributed to the production of a thermal residual stress during the plasma spraying. Additional analysis of crack generation and lifetime performance with the layered TBC system through TGMF tests will be covered further in the future work.

It should be noted that there are a few limitations in the current work. In this work, due to limited number of samples, we were unfortunately unable to conduct sufficient tests to systematically analyze the initiation and propagation of cracks. Ideally, the crack initiation and propagation phenomena among the samples can be captured through interruption at various thermal cycles. These limitations should be addressed in the future work.

4. Conclusions

The lifetime performance of YGYZ-based TBCs with a buffer layer was investigated through the TGMF test with two different thermal cycling frequency conditions, and the following conclusions are obtained.

1. Although both the high- and low- thermal cycling frequency TBC samples survived the TGMF tests with the same test period (total 5000 mins), the high-frequency samples demonstrated a better durability based on microstructural analysis. This is due to the fact that less temperature change and the associated residual stress were generated in the high-frequency samples than the low-frequency ones.

2. Thermal cycling frequency causes different crack generation modes with different lengths and quantities of the vertical cracks. In the low-frequency cycling TGM test, the long heating period caused a higher temperature difference and high residual stress that generated a few penetrating vertical cracks. In contrast, in the high-frequency cycling TGMF test, the YGYZ-top coat was subject to less temperature change and residual stress, causing multiple narrow vertical cracks.

3. The samples with the HP-YSZ buffer layer have a better thermal and mechanical durability in low-frequency TGMF test. The YSZ buffer layer prevented the propagation of the vertical cracks towards the interface between the top and bond coats, through reducing their CTE mismatch. For the low-frequency test, some fine cracks were generated in the both RP- and HP-YSZ buffer layers. Even if some vertical cracks were generated in the RP-YSZ buffer layer, it is difficult to tell the difference through the microstructural examination. For the high-frequency test, the difference between the HP-YSZ and RP-YSZ is less evident, since the generated vertical cracks were far away from the buffer layer.

4. A finite element model is developed, which takes creep effect into account due to thermal cycling. The model shows the high stresses at the interfaces between different layers due to differential thermal expansion.

5. The crack initiation and propagation behaviors in both frequencies are

controlled by the direction of the generated tensile load in the coatings. The vertical cracks were the primary fracture features in the TGMF tests. The vertical cracks were created on the top surface during the TGMF test, and then propagated towards to the interface between the top coat and the buffer layer. The transverse cracks then propagated when the vertical cracks were impeded by pores and micro-cracks at the interface where residual stress was present. These cracks finally resulted in the spallation of the ceramic coating when the transverse cracks were connected to each other.

Acknowledgments

This work was supported by "Human Resources Program in Energy Technology" of the Korea Institute of Energy Technology Evaluation and Planning (KETEP), granted financial resource from the Ministry of Trade, Industry & Energy, Republic of Korea (No. 20174030201460) and by Fundamental Research Program of the Korean Institute of Materials Science (KIMS, No. PNK5620).

References

[1] R.A. Miller, Current status of thermal barrier coatings—an overview, Surf. Coat. Technol. 30 (1987) 1-11.

[2] D.R. Clarke, M. Oechsner, N.P. Padture, Thermal-barrier coatings for more efficient gas-turbine engines, MRS bulletin, 37 (2012) 891-898.

[3] N.P. Padture, M. Gell, E.H. Jordan, Thermal barrier coatings for gas-turbine engine applications, Science. 296 (2002) 280-284.

[4] R. Kitazawa, M. Tanaka, Y. Kagawa, Y.F. Liu, Damage evolution of TBC system under in-phase thermo-mechanical tests, 173 (2010) 130-134

[5] R. Trice, Y.J. Su, J. Mawdsley, K. Faber, A. De Arellano-Lopez, H. Wang, W. Porter, Effect of heat treatment on phase stability, microstructure, and thermal conductivity of plasma-sprayed YSZ, J. Mater. Sci. 37 (2002) 2359-2365.

[6] T. Totemeier, W. Gale, J. King, Isothermal fatigue of an aluminide-coated single-crystal superalloy: Part II. effects of brittle precracking, Metall. Mater. Trans. A, 27 (1996) 363-369.

[7] R. Vassen, A. Stuke, D. Stöver, Recent developments in the field of thermal barrier coatings, J. Therm. Spray Technol. 19

(2009) 181-186.

[8] D. Stöver, G. Pracht, H. Lehmann, M. Dietrich, J.-E. Döring, R. Vassen, New material concepts for the next generation of plasma-sprayed thermal barrier coatings, J. Therm. Spray Technol. 13 (2004) 76-83.

[9] A. Karaulov, E. Zoz, Phase formation in the ZrO_2-HfO_2-Gd_2O_3 and ZrO_2-HfO_2-Yb_2O_3 systems, Refract. Ind. Ceram. 40 (1999) 479-483.

[10] C.G. Levi, Emerging materials and processes for thermal barrier systems, Curr. Opin. Solid State Mater. Sci. 8 (2004) 77-91.

[11] X. Guo, Z. Lu, Y.-G. Jung, L. Li, J. Knapp, J. Zhang, Thermal properties, thermal shock, and thermal cycling behavior of lanthanum zirconate-based thermal barrier coatings, Metall. Mater. Trans. E. 3 (2016) 64-70.

[12] B.T. Richards, S. Sehr, F. de Franqueville, M.R. Begley, H.N. Wadley, Fracture mechanisms of ytterbium monosilicate environmental barrier coatings during cyclic thermal exposure, Acta Materialia, 103 (2016) 448-460.

[13] S. Lakiza, O. Fabrichnaya, C. Wang, M. Zinkevich, F. Aldinger, Phase diagram of the ZrO_2–Gd_2O_3–Al_2O_3 system, J. Eur. Ceram. Soc. 26 (2006) 233-246.

[14] Z.G. Liu, J.-H. Ouyang, Y. Zhou, Preparation and thermophysical properties of $(Nd_xGd_{1-x})_2Zr_2O_7$ ceramics, J. Mater. Sci. 43 (2008) 3596-3603.

[15] J. Feng, B. Xiao, C. Wan, Z. Qu, Z. Huang, J. Chen, R. Zhou, W. Pan, Electronic structure, mechanical properties and thermal conductivity of $Ln_2Zr_2O_7$ (Ln= La, Pr, Nd, Sm, Eu and Gd) pyrochlore, Acta Materialia, 59 (2011) 1742-1760.

[16] L. Guo, H. Guo, H. Peng, S. Gong, Thermophysical properties of Yb_2O_3 doped Gd2Zr2O7 and thermal cycling durability of $(Gd_{0.9}Yb_{0.1})_2Zr_2O_7$/YSZ thermal barrier coatings, J. Eur. Ceram. Soc. 34 (2014) 1255-1263.

[17] J. Singh, D.E. Wolfe, J. Singh, Architecture of thermal barrier coatings produced by electron beam-physical vapor deposition (EB-PVD), J. Mater. Sci. 37 (2002) 3261-3267.

[18] R. Vassen, F. Traeger, D. Stöver, New Thermal Barrier Coatings Based on Pyrochlore/YSZ Double- Layer Systems, Int. J. Appl. Ceram. Technol. 1 (2004) 351-361.

[19] J. Thornton, A. Majumdar, G. McAdam, Enhanced cerium migration in ceria-stabilised zirconia, Surf. Coat. Technol. 94 (1997) 112-117.

[20] X. Cao, R. Vassen, D. Stoever, Ceramic materials for thermal barrier coatings, J. Eur. Ceram. Soc. 24 (2004) 1-10.

[21] Takeoff with advanced coatings, Sulzer Technical Rev. 3 (2013) 8-12, https://www.oerlikon.com/ecomaXL/files/metco/oerlikon_STR_3_08_12_Dorfman.pdf&download=1.

[22] Material Product Data Sheet, https://www.oerlikon.com/ecomaXL/files/metco/oerlikon_DSMTS-0001.10_8YO_ZrO_HOSP.pdf&download=1.

[23] Y. Radin, T. Kontorovich, Equivalent operating hours concept for ccpp components reliability evaluation, 2012 International Conference on Power Energy System, 2012, pp. 175-178.

[24] T. Clyne, S. Gill, Residual stresses in thermal spray coatings and their effect on interfacial adhesion: a review of recent work, J. Therm. Spray Technol. 5 (1996) 401.

[25] S.R. Choi, D. Zhu, R.A. Miller, Mechanical Properties/Database of Plasma-Sprayed ZrO_2-8wt% Y_2O_3 Thermal Barrier Coatings, International J. Appl. Ceram. Technol. 1 (2004) 330-342.

[26] M. Bartsch, G. Marci, K. Mull, C. Sick, Fatigue testing of ceramic thermal barrier coatings for gas turbine blades, Adv. Eng. Mater. 1 (1999) 127-129.

[27] M. Bartsch, B. Baufeld, S. Dalkilic, L. Chernova, M. Heinzelmann, Fatigue cracks in a thermal barrier coating system on a superalloy in multiaxial thermomechanical testing, Int. J. Fatigue, 30 (2008) 211-218.

[28] G. Lyu, B.G. Kim, S.S. Lee, Y.G. Jung, J. Zhang, B.G. Choi, Fracture behavior and thermal durability of lanthanum zirconate-based thermal barrier coatings with buffer layer in thermally graded mechanical fatigue environments, Sur. Coat. Technol.332 (2017) 64-71.

[29] R.A. Miller, C.C. Berndt, Performance of thermal barrier coatings in high heat flux environments, Thin Solid Films, 119 (1984) 195-202.

[30] R. Vassen, X. Cao, F. Tietz, D. Basu, D. Stöver, Zirconates as new materials for thermal

barrier coatings, J. Am. Ceram. Soc. 83 (2000) 2023-2028.

[31] E. Bakan, D.E. Mack, G. Mauer, R. Vassen, Gadolinium zirconate/YSZ thermal barrier coatings: plasma spraying, microstructure, and thermal cycling behavior, J. Am. Ceram. Soc. 97 (2014) 4045-4051.

[32] S.H. Jung, Z. Lu, Y.G. Jung, D. Song, U. Paik, B.G. Choi, I.S. Kim, X. Guo, J. Zhang, Thermal durability and fracture behavior of layered Yb-Gd-Y-based thermal barrier coatings in thermal cyclic exposure, Surf. Coat. Technol. 323 (2017) 39-48.

[33] D. Song, U. Paik, X. Guo, J. Zhang, T.-K. Woo, Z. Lu, S.-H. Jung, J.-H. Lee, Y.-G. Jung, Microstructure design for blended feedstock and its thermal durability in lanthanum zirconate based thermal barrier coatings, Surf. Coat. Technol. 308 (2016) 40-49.

[34] K.-Y. Park, Y.-G. Jung, I.-S. Kim, B.I. Yang, Effects of Purity and Phase Content of Feedstock Powder on Thermal Durability of Zirconia-Based Thermal Barrier Coatings, (6)26 (2017) 1161-1167.

[35] L. Wang, Y. Wang, X. Sun, J. He, Z. Pan, C. Wang, Thermal shock behavior of 8YSZ and double-ceramic-layer $La_2Zr_2O_7$/8YSZ thermal barrier coatings fabricated by atmospheric plasma spraying, Ceram. Int. 38 (2012) 3595-3606.

Table caption

Table. 1. Summary of the number of cycles and exposure time in the TGMF tests

Figure captions

Fig. 1. Side and surface photographs of the sample used in the TGMG test.

Fig. 2. Morphology of feedstock powders: (A) YGYZ, (B) low-purity YSZ and (C) high-purity YSZ.

Fig. 3. Schematic illustration of layered TBCs: (A) YGYZ-based TBC with a buffer layer of RP-YSZ and (B) YGYZ-based TBC with a buffer layer of HP-YSZ.

Fig. 4. Experimental apparatus and conditions in the TGMF test: (A) side view of the TGMF apparatus, (B) front view of the tested samples in TGMF test.

Fig. 5. Experimental conditions in the TGMF test: (A) schematic diagram for observing microstructure with the flame position and the loading direction, (B) low-frequency cycling, and (C) high-frequency cycling. Solid and dotted lines indicate the measured temperature on the top surface of the sample and the scheduled temperature, respectively.

Fig. 6. As-prepared microstructures of layered TBCs: (A) YGYZ-based TBC with a buffer layer of RP-YSZ and (B) YGYZ-based TBC with a buffer layer of HP-YSZ. Each number indicates the whole microstructure, top coat, interface of top coat and buffer layer, and interface of buffer layer and bond coat

Fig. 7. Microstructures of layered TBCs after the TGMF test: (A) YGYZ-based TBC with a buffer layer of RP-YSZ and (B) YGYZ-based TBC with a buffer layer of HP-YSZ. Each number indicates the low- and high-frequency cycling, respectively.

Fig. 8. Microstructures of layered TBCs after low-frequency cycling in the TGMF test: (A) YGYZ-based TBC with a buffer layer of RP-YSZ and (B) YGYZ-based TBC with a buffer

layer of HP-YSZ. Each number indicates the whole microstructure, top coat, interface of top coat and buffer layer, and interface of buffer layer and bond coat.

Fig. 9. Microstructures of layered TBCs after high-frequency cycling in the TGMF test: (A) YGYZ-based TBC with a buffer layer of RP-YSZ and (B) YGYZ-based TBC with a buffer layer of HP-YSZ. Each number indicates the whole microstructure, top coat, interface of top coat and buffer layer, and interface of buffer layer and bond coat.

Fig. 10: Finite element model of the TBC. Due to axial symmetry, only a half cross-section with axial symmetric finite element is used.

Fig. 11: von Mises stress (unit: Pa) distributions in the TBCs (two third of the coatings are shown to illustrate both the interior and exterior regions): (a) low-frequency sample, (b) high-frequency sample.

Fig. 12: Effective creep strain (in log scale) evolution at the outer edge of the YGYZ and YSZ interface: (a) low-frequency sample, (b) high-frequency sample.

Fig. 13. Schematic illustration of the crack propagation model: (A) YGYZ-based TBC under low-frequency cycling and (B) YGYZ-based TBC under high-frequency cycling

Table 1. Summary of the number of thermal cycles and exposure time in the TGMF tests

Sample species (Top coat/buffer layer)	Cycling frequency	Test (cycles)	Exposure time (min)
(A) YGYZ/RP-YSZ	Low-frequency	1,000	10,000
(B) YGYZ/HP-YSZ	Low-frequency	1,000	10,000
(C) YGYZ/RP-YSZ	High-frequency	5,000	10,000
(D) YGYZ/HP-YSZ	High-frequency	5,000	10,000

Research Highlights

- Yb-Gd-Y-stabilized zirconia (YGYZ) based TBCs with buffer layer was well prepared.
- Thermal cycling frequency caused different crack growth behavior in TGMF test.
- HP-YSZ buffer layer showed a better thermal durability in low-frequency TGMF test.
- A finite element model showed the high stresses at the interfaces between different layers.
- The failure mechanisms of YGYZ-based TBCs in TGMF test were proposed.

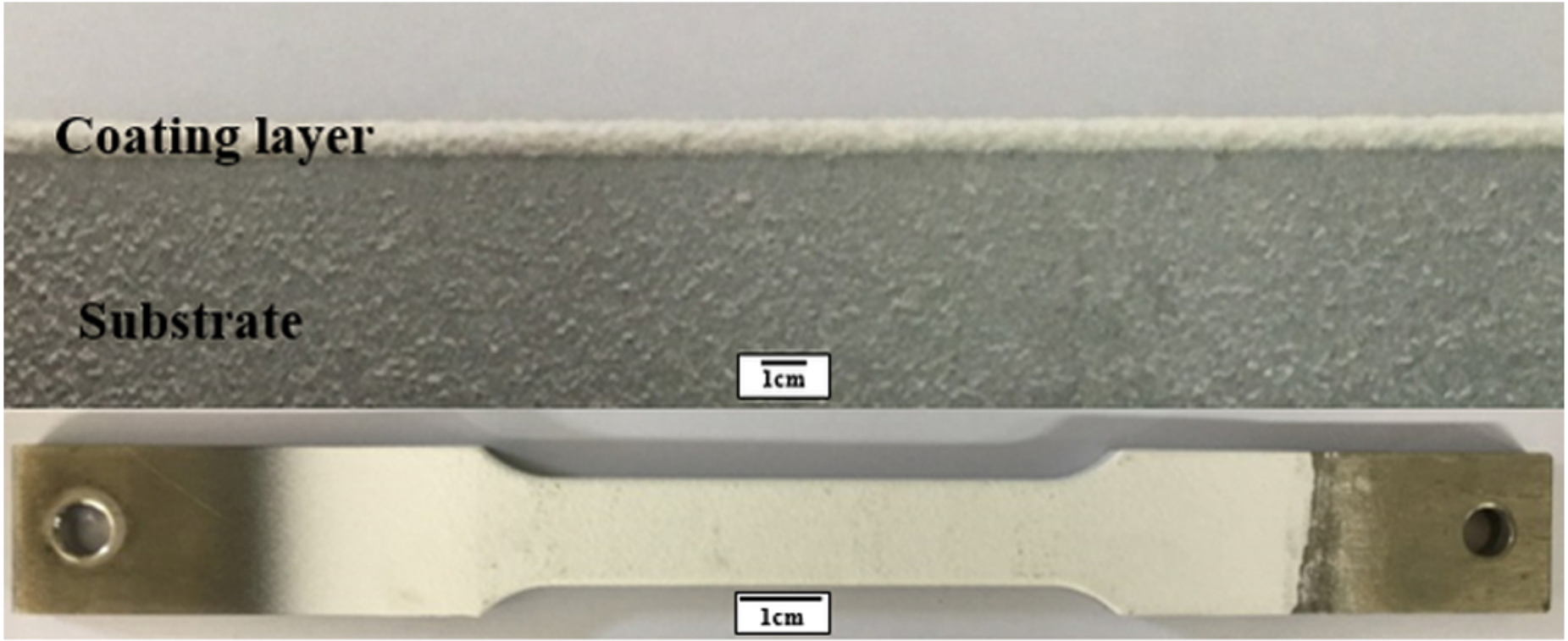

Figure 1

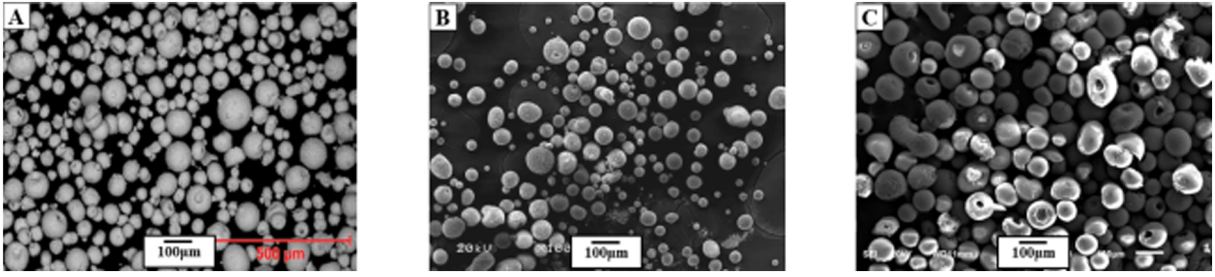

Figure 2

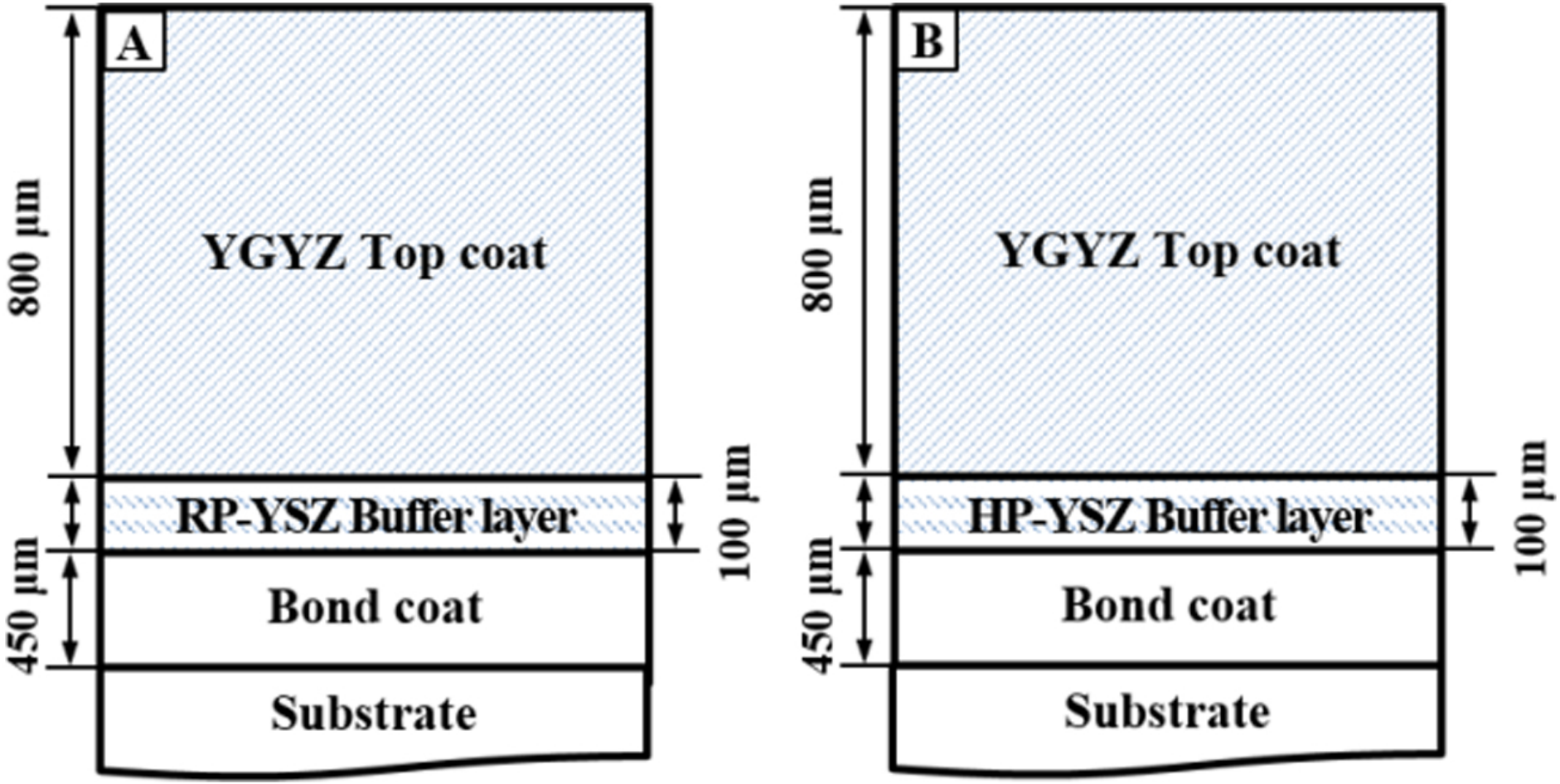
A
YGYZ Top coat
800 µm
RP-YSZ Buffer layer
100 µm
450 µm
Bond coat
Substrate
B
YGYZ Top coat
800 µm
HP-YSZ Buffer layer
100 µm
450 µm
Bond coat
Substrate

Figure 3

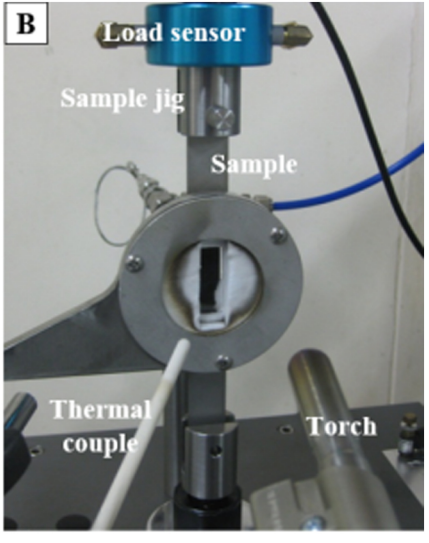

Figure 4

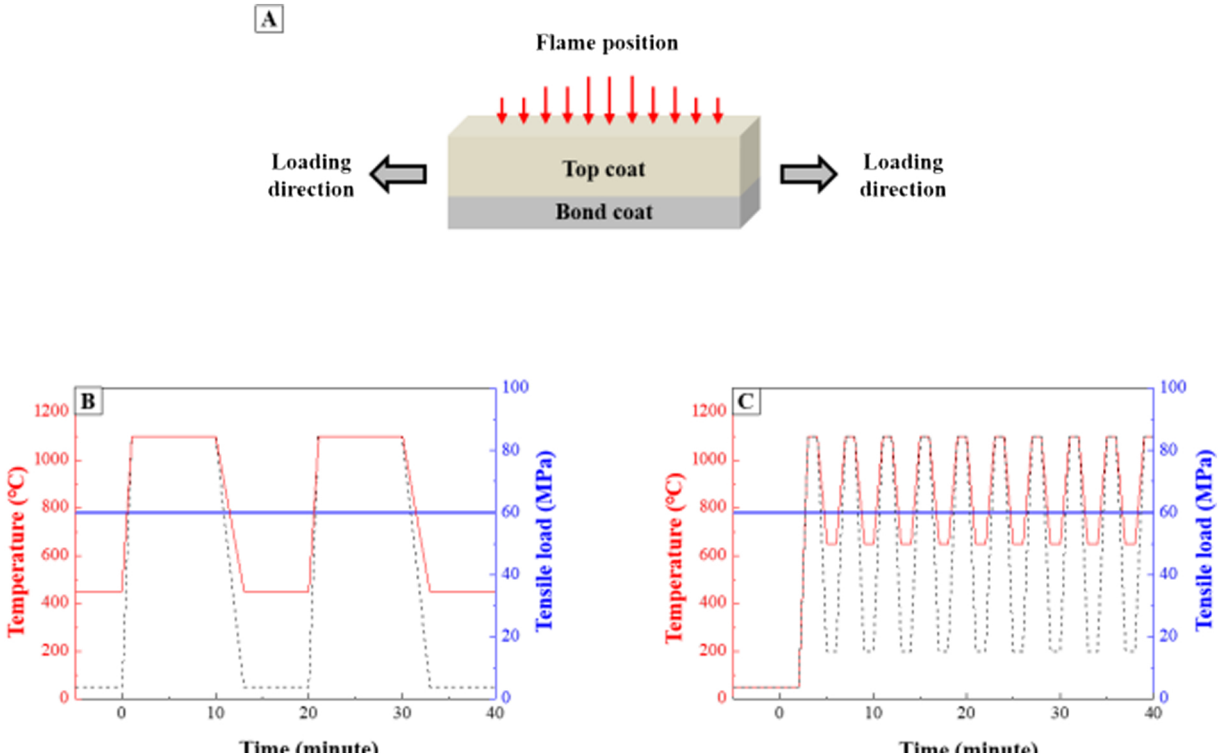
A
Flame position
Loading direction
Top coat
Bond coat
Loading direction
B
Temperature (°C)
Tensile load (MPa)
Time (minute)
C
Temperature (°C)
Tensile load (MPa)
Time (minute)

Figure 5

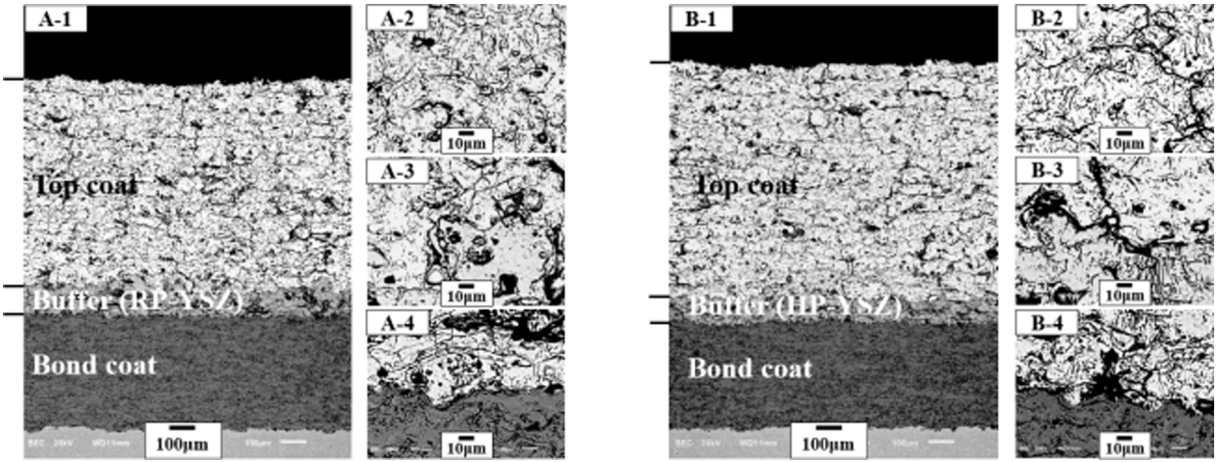
A-1
A-2
A-3
A-4
Top coat
Buffer (RP-YSZ)
Bond coat
100μm
10μm
10μm
10μm
B-1
B-2
B-3
B-4
Top coat
Buffer (HP-YSZ)
Bond coat
100μm
10μm
10μm
10μm

Figure 6

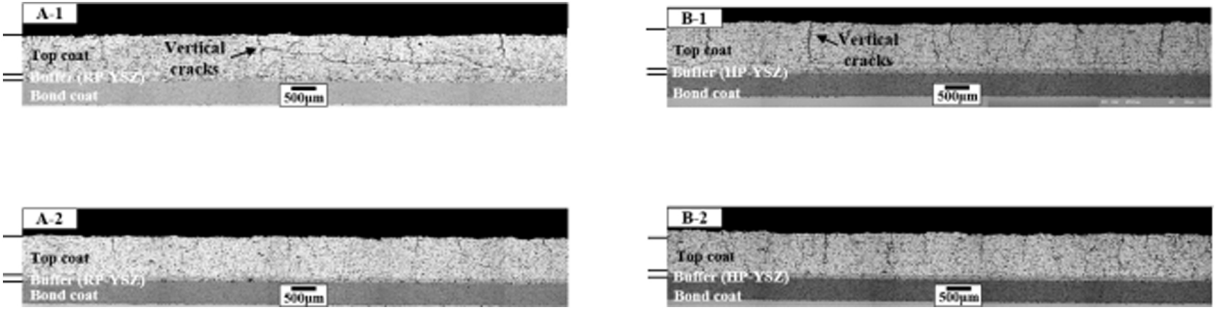
A-1
Top coat
Vertical cracks
Buffer (RP-YSZ)
Bond coat
500μm
B-1
Top coat
Vertical cracks
Buffer (HP-YSZ)
Bond coat
500μm
A-2
Top coat
Buffer (RP-YSZ)
Bond coat
500μm
B-2
Top coat
Buffer (HP-YSZ)
Bond coat
500μm

Figure 7

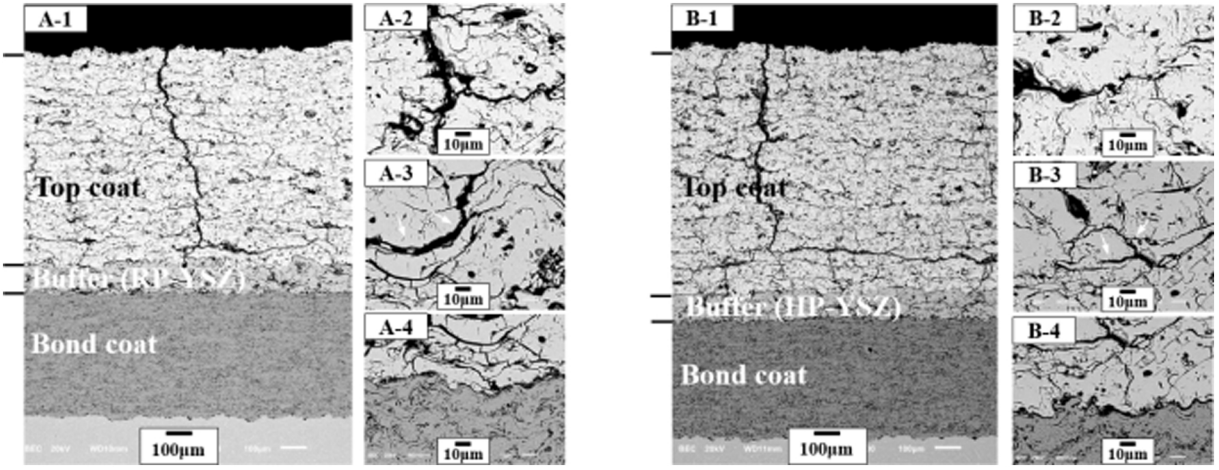
A-1
Top coat
Buffer (RP-YSZ)
Bond coat
100μm
A-2
10μm
A-3
10μm
A-4
10μm
B-1
Top coat
Buffer (HP-YSZ)
Bond coat
100μm
B-2
10μm
B-3
10μm
B-4
10μm

Figure 8

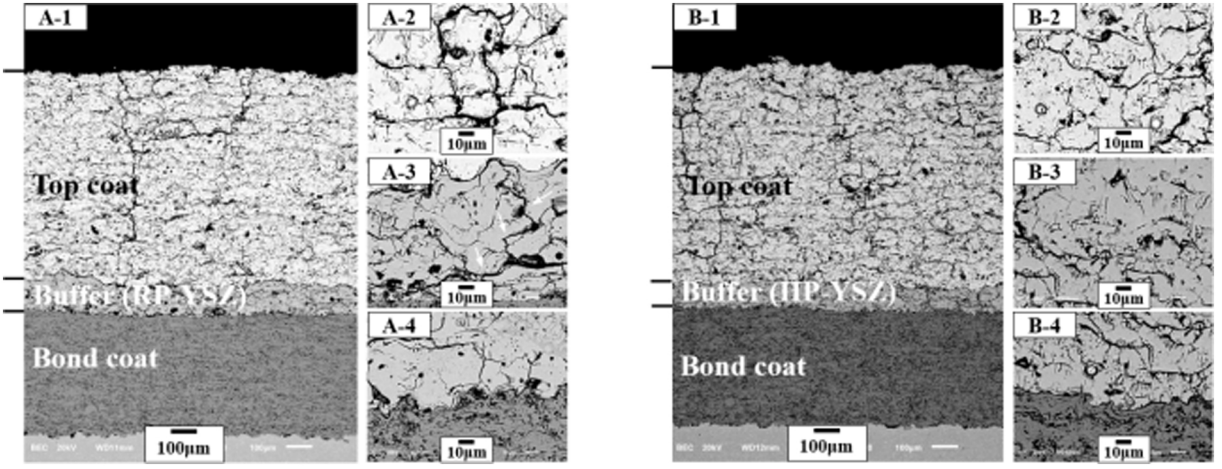
A-1
A-2
A-3
A-4
Top coat
Buffer (RP-YSZ)
Bond coat
100μm
10μm
B-1
B-2
B-3
B-4
Top coat
Buffer (HP-YSZ)
Bond coat
100μm
10μm

Figure 9

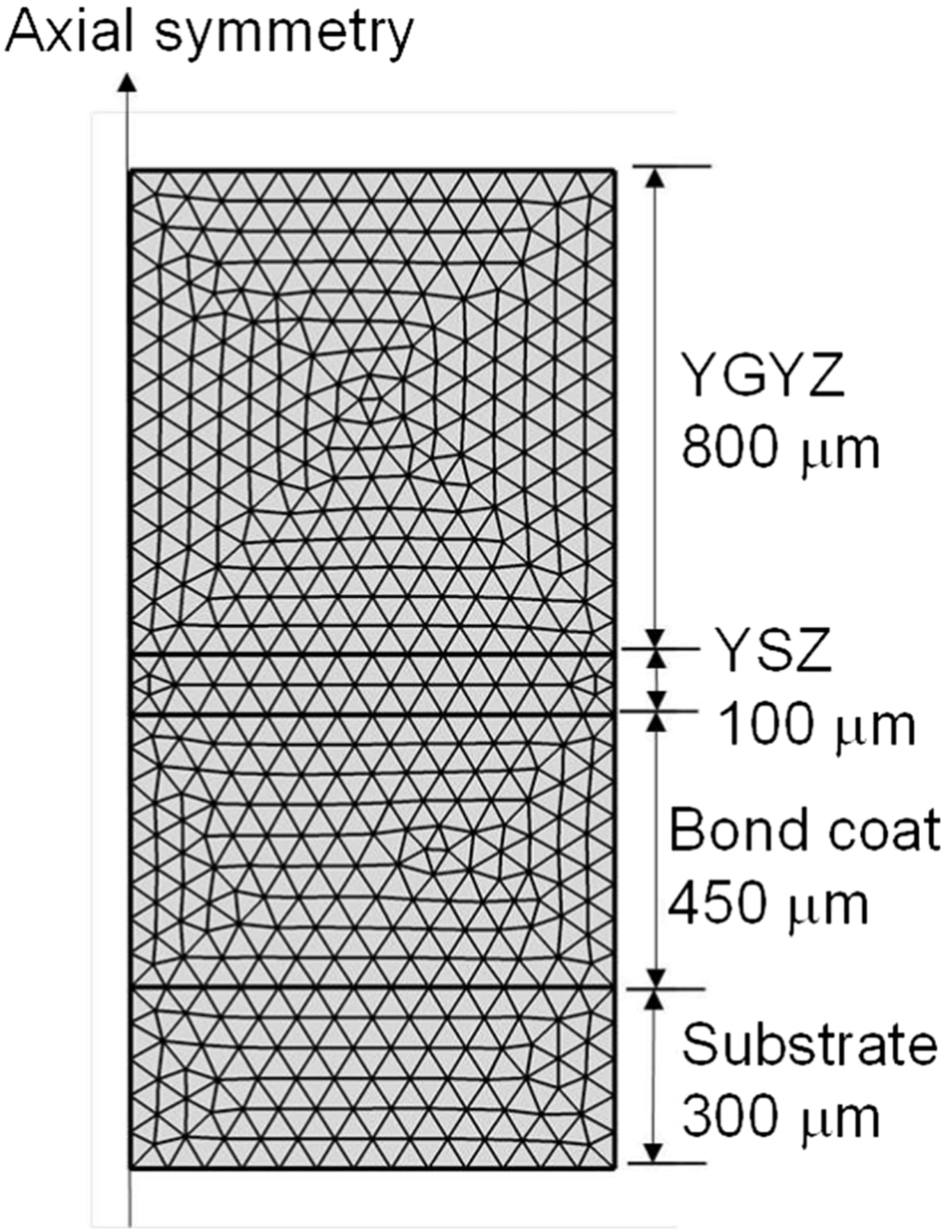
Axial symmetry
YGYZ
800 μm
YSZ
100 μm
Bond coat
450 μm
Substrate
300 μm

Figure 10

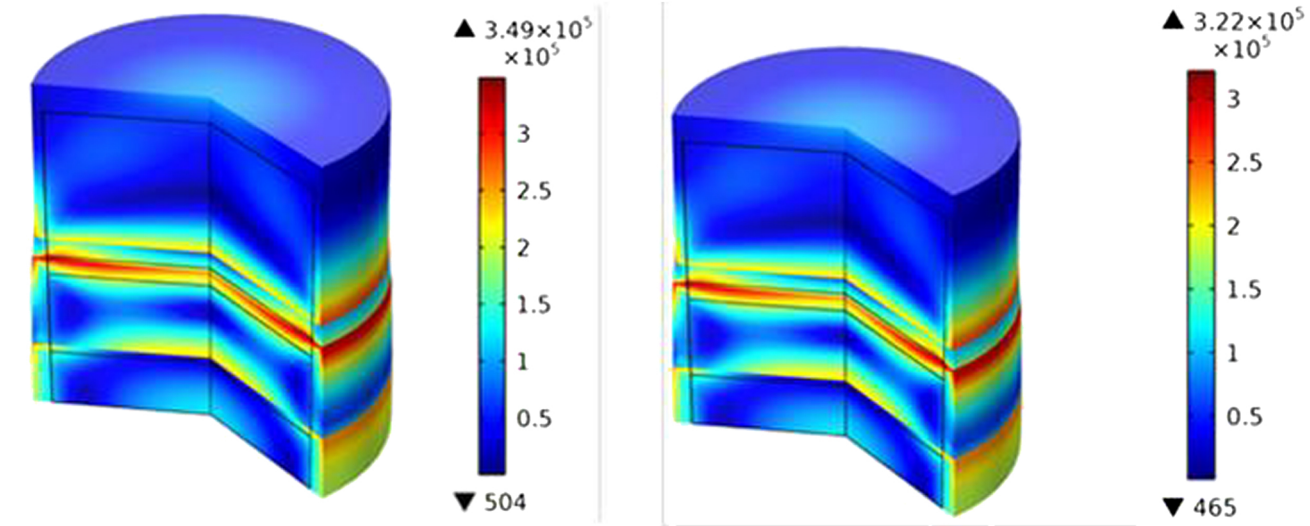

Figure 11

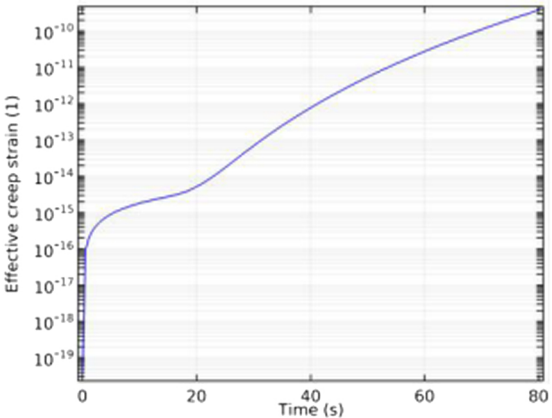
Effective creep strain (1)
10^-10
10^-11
10^-12
10^-13
10^-14
10^-15
10^-16
10^-17
10^-18
10^-19
0
20
40
60
80
Time (s)

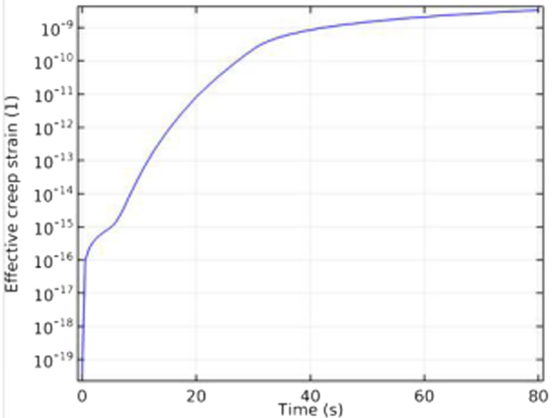
Effective creep strain (1)
10^-9
10^-10
10^-11
10^-12
10^-13
10^-14
10^-15
10^-16
10^-17
10^-18
10^-19
0
20
40
60
80
Time (s)

Figure 12

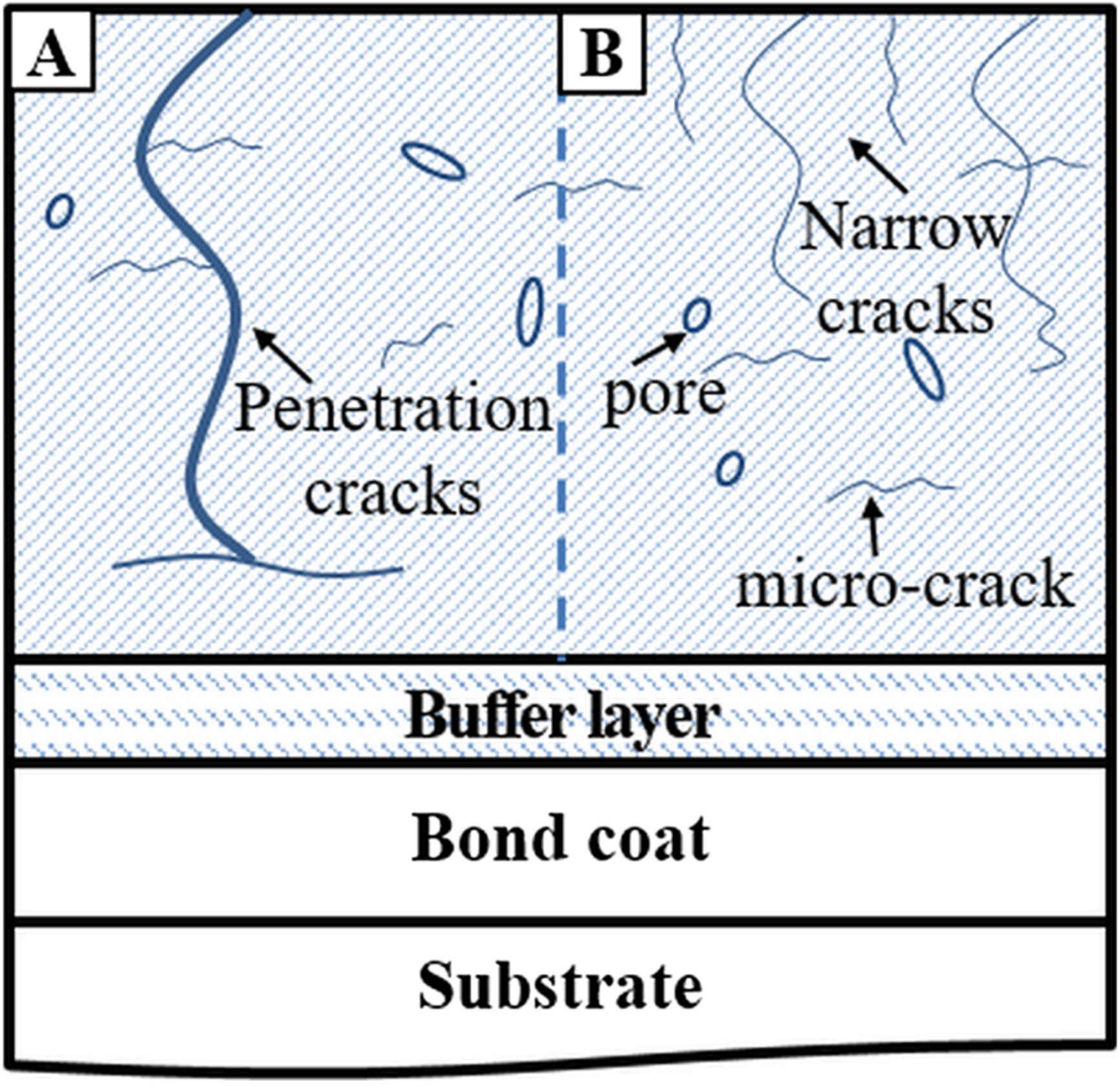
A
B
Narrow
cracks
Penetration
cracks
pore
micro-crack
Buffer layer
Bond coat
Substrate

Figure 13